

Micro/Nanotribological studies of silicon and CN_x coatings: Crystallography-induced anisotropy in friction and seizure

Philippe Stempflé and Jamal Takadoum

Institut FEMTO-ST (UMR CNRS 6174 – Université de Franche Comté – CNRS – ENSMM – UTBM)

ENSMM, 26 Chemin de l'Épitaphe F-25030 Besançon Cedex, France

philippe.stempfle@ens2m.fr

Abstract: The micro/nanotribological behaviour of various monocrystalline silicon wafers – displaying various orientations and roughnesses – rubbing on metals and ceramics balls are investigated under multi-asperity low contact pressures. Whatever the antagonist, results reveal a crystallography-induced anisotropy in friction due to crystallographic orientation of the wafer. This anisotropy leads to a time-dependent seizure mechanism – connected to the surface energy of the wafer itself linked to its crystal orientation. The wafer roughness mainly influences the generation rate of the third body and finally controls the seizure mechanism. When CN_x coatings are deposited on wafer, anisotropy does completely vanish: friction and wear mechanisms are instead controlled by the surrounding environment.

Key words: Micro/Nanotribology ; Monocrystalline silicon wafer ; Nitride Carbide coatings

1. INTRODUCTION

Currently, friction and wear processes of small contact surfaces met in the micro-mechanical devices (so-called MEMS) are still largely misunderstood [1-5]. Indeed, designed to small tolerances, reliability of MEMS devices (comb drives, grippers, motors, gear trains [4,6]) is strongly affected by various surface phenomena as friction/stiction [6-9], micro- and nanoscopic wear [10-12], surface contamination and environmental effects [13-16]. Although the apex of the AFM is commonly used to simulate and study these phenomena [17-20], it is generally admitted that the friction level and wear rate obtained with this approach – *i.e* on the scale of a single asperity contact – have little to do with the ones obtained in microsystems [1,2,5,6,11,15,16,21-25]. Indeed,

a single asperity can not take into account the mutual interaction coming from all neighbouring contacts and, the comprehension of mechanisms that contribute to the overall view of friction is generally insufficient – *i.e* the scale dependence of friction [21], the influence of the environment [15], the thermal effects [26], the physico-chemical interactions and/or the formation of third body within the contact [*eg.* 27]. In addition, the level of contact pressure in that configuration is often much higher than real MEMS (several GPa) leading to study phenomena which can be completely different than those really occurring in current microsystems.

Thus, the aim of this paper is to study friction and wear mechanisms occurring on the micro/nanoscale level by considering a multi-asperity contact under low contact pressures (several MPa). As an excellent structural material, single-crystalline silicon wafer is commonly used

in MEMS devices. Besides, many studies have been devoted to its tribological behaviour - mainly during the early cycles of sliding – in respectively single [1-4,7,10,14,17-20] and multi-asperity contact configuration [2,5,6,8,11,15,16,21-24, 28,29,31]. Referring to literature, monocrystalline Si(100) or Si(110) wafers have been widely more studied than Si(111) – the ratio is about 2/10 – because the micro/nanomanufacturing techniques for MEMS devices are clearly suitable for these crystallographic orientations (*e.g.* bulk micromachining or surface micromachining) [4]. However, it is well known that Si (111) displays simultaneously better mechanical properties [29-33] and a weaker surface energy [28, 31, 34] than Si(100) and Si(110) orientations. Anyway, micro/nanotribological problems in MEMS are usually solved by using either hard coatings [3,6,8,12,24,35,38] or molecularly thin fluid films or gas phase lubrication [*eg.* 37] whereas the effect of crystallographic orientation of the silicon planes in absence and presence of coatings is not completely investigated yet.

In this work, the tribological behaviour will be studied by varying: (i) the size and the materials constituting the pin (*metals* or *ceramics*); (ii) the roughness and the crystallographic orientation of the monocrystalline silicon samples; (iii) the presence of coatings like carbon nitride coatings [35, 36].

2. EXPERIMENTAL SETUP

2.1. Tribological setup

The experimental device is constituted by a ball-on-disc *nanotribometer* manufactured by *CSM Instruments (Switzerland)*. A pin is mounted on a stiff lever, designed as a frictionless force transducer ($K_x = 265\text{Nm}^{-1}$; $K_z = 152.2\text{Nm}^{-1}$). The friction force is determined during the test by measuring the deflection of the elastic arm (low load range down to $50\mu\text{N}$). The ball is loaded onto a flat sample with a precisely known force using

closed loop. The load and friction resolutions are about $1\mu\text{N}$.

In this work, tribological tests are carried out in linear reciprocating mode at room temperature (22°C) under ambient air (RH 35%). The normal load varies from 10 to 80mN corresponding to a contact pressure varying from 0.15-0.65GPa according to the size and the materials constituting the ball. The stroke frequency, the stroke length and the stroke length resolution are respectively 10Hz, $\pm 0.5\text{mm}$, and 250nm. The velocity and the sliding distance are respectively 1mms^{-1} and 0.2m corresponding to 100 cycles.

A real-time depth measuring sensor is used for studying the time dependent wear properties. The depth range varies from 20nm to $100\mu\text{m}$ with a resolution of about 20nm. Results are then compiled using a triboscopic approach [37] (see fig 2 for instance) giving simultaneously and for each cycle : (i) the evolution of the friction coefficient along the friction track (*friction map* fig 2a) and, (ii) the evolution of the ball depth within the friction track (*depth map* fig 2b). The latter revealing any time-dependent wear process and/or potential build-up of a tribolayer within the contact.

2.2. Samples

Five types of flat samples were selected for the present study: a rough single crystal silicon (100) wafer ($R_a: 685\text{nm}$); a polished single crystal silicon (100) wafer ($R_a: 0.311\text{nm}$); a polished single crystal (111) wafer ($R_a: 0.244\text{nm}$); and two $2.8\pm 0.5\mu\text{m}$ carbon nitride (CN_6) coatings deposited on respectively polished monocrystal (100) and (111) silicon wafers ($R_a: 0.355\text{nm}$) by using PE-CVD technique. Details of the coatings process are available in [35]. Silicon monocrystals are n-type material grown by CZ process and p-doped. To simulate the real surface of MEMS, the native oxide layer on silicon surface (thickness: $\cong 0.5\text{nm}$) was not removed by any chemical method.

Balls are made of metals (100Cr6) or ceramics (Si_3N_4 , Al_2O_3) in order to change the surface interactions with the flat samples. They display various diameters ($\varnothing 1.5$ and $\varnothing 4\text{mm}$) to take into

account the scale dependence of friction [21]. For each type of ball, the contact pressure is computed using a Hertzian model. Table 1 compiles the mechanical properties of each sample.

3. RESULTS & DISCUSSION

3.1. Tribological tests on rough single crystal silicon (100) wafers

Fig.1 plots the variations of the friction coefficient – after 100 cycles – as a function of the contact pressure for each type of ball rubbing on rough Si(100) wafers (greatest diameters corresponding to lowest contact pressures).

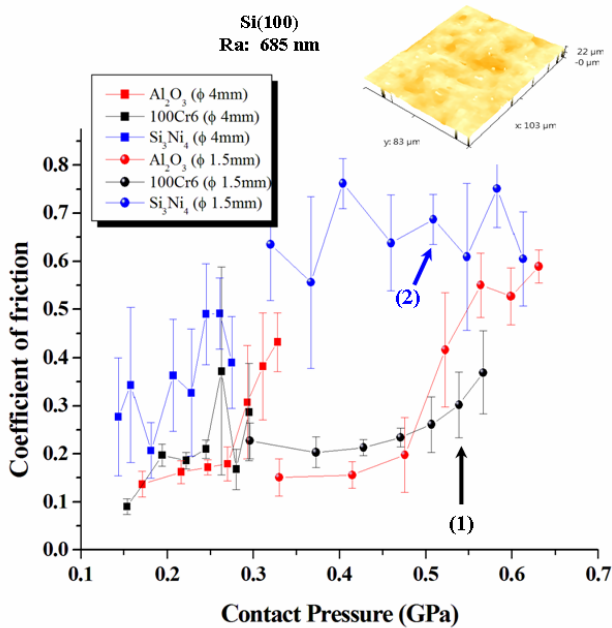


Fig 1: Variations of the friction coefficient vs. contact pressure in the case of rough monocrystal Si(100) wafers

A strong influence of the material constituting the ball is observed. Thus, in spite of their apparent inertness ceramic balls always lead to seizure phenomena in contrast to metal balls. The alumina seizure threshold is even much higher than the silicon nitride one revealing that this latter is certainly more reactive with the silicon than alumina, as recently reported by Achanta *et al* [6]. However, alumina is clearly subjected to a ball

size effect (around 0.3 GPa) leading to a drop in the friction coefficient when the size of the ball changes.

	Si(100)	Si(111)	100Cr6	Si ₃ N ₄	Al ₂ O ₃
E (GPa)	129	187	210	310	370
ν	0.28	0.36	0.3	0.22	0.21

Table 1: Mechanical properties of the samples [36]

For a better understanding of these various tribological behaviours, an *in situ* triboscopic approach is used for the tests showed by arrows (1) and (2) in fig 1. Let us point out that this approach gives simultaneously and for each cycle (fig. 2): (i) the evolution of the friction coefficient along the friction track and, (ii) the evolution of the ball depth (in μm) within the friction track. Thus for the metal ball – arrow (1) shown in fig.1 – the *friction map* (fig 2a) is rather stable vs. cycles while the *depth map* reveals a time-dependent build-up of a tribolayer constituted by agglomerated wear debris within the contact. The presence of the tribolayer is confirmed by the SEM map of the wear groove after 100 cycles (fig 2c). Enlargement (fig 2d) reveals that the tribolayer is not really cohesive: debris are compacted at the tips of the groove increasing the friction coefficient at both tracks ends (fig 2a) .

In contrast for the ceramic ball - arrow (2) in fig.1 - seizure is observed halfway (Fig 3a). However, the sliding length before seizure strongly depends on the contact pressure: the higher the contact pressure the lower the length before seizure. Besides, seizure is instantaneous when the contact pressure reaches 0.65 GPa. As shown on the *depth map* (fig 3b), seizure induces a widening of the friction groove. In this case, seizure is observed because the third body does not stay within the contact area and is mainly ejected out of the wear groove.

Concerning the increase in the alumina friction coefficient at low contact pressures (fig 1, under 0.3 GPa), corresponding triboscopic results revealed that it was only due to the presence of a more significant amount of cohesive third body under the large ball than under the small one.

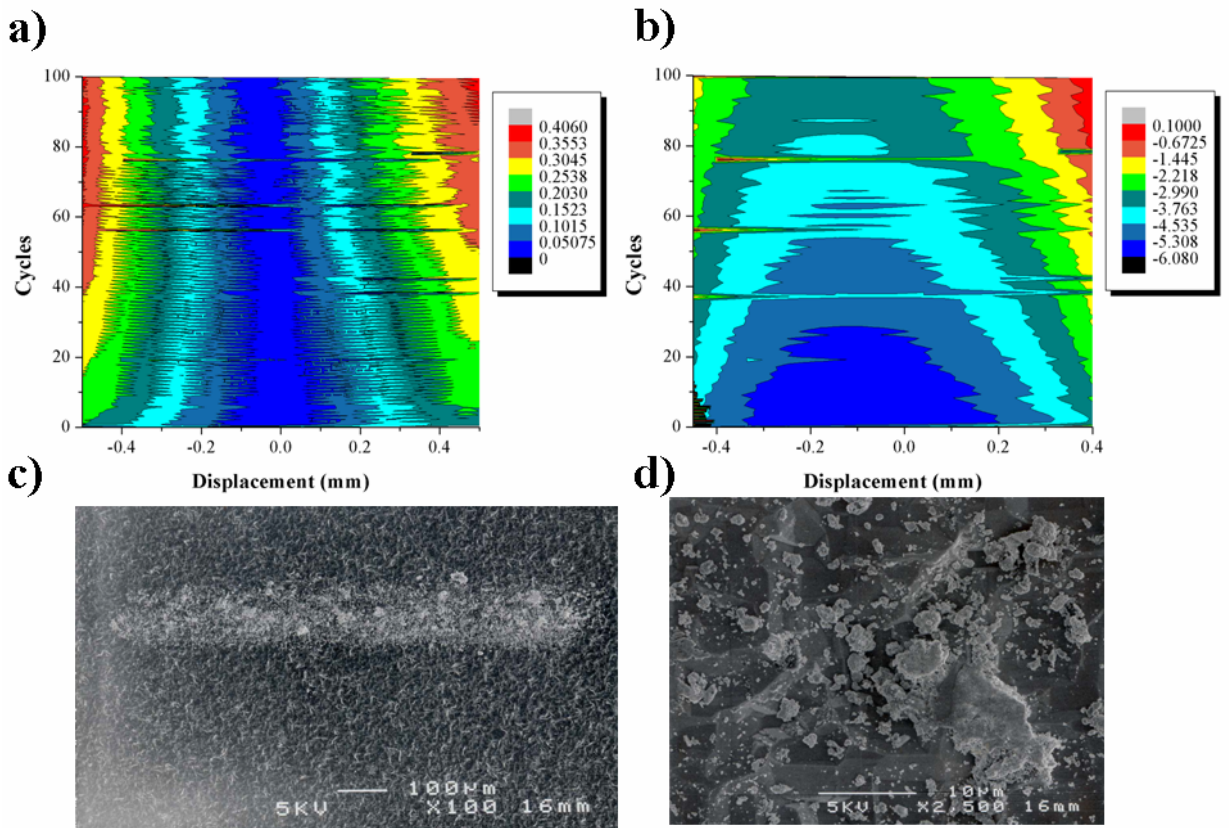


Fig 2: Triboscopic views of the test corresponding to arrow (1) in fig 1: friction map (a) ; depth map in μm (b) ; and SEM view of the wear groove (c) and wear debris (d)

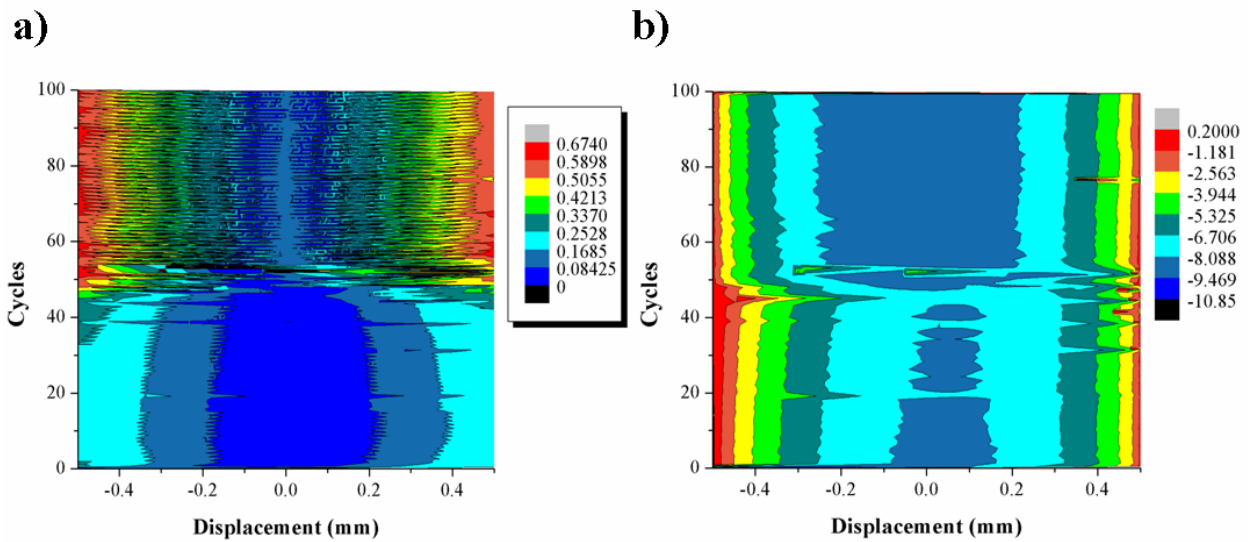


Fig 3: Triboscopic views of the test corresponding to arrow (2) in fig 1 : friction map (a) ; depth map in μm (b)

3.2. Tribological tests on polished single crystal silicon (100) wafers

Fig. 4 plots the variations of the friction coefficient – after 100 cycles – as a function of the contact pressure for each type of ball rubbing on polished Si(100) wafers.

For the lowest contact pressures, friction coefficient is independent of the materials constituting the balls. At the highest contact pressures, and in contrast to previous results (fig 1), seizure is always observed whatever the antagonist. However, the seizure threshold is two times greater for ceramics (0.6 GPa) than metals (0.3 GPa). In addition, both ceramic behaviours are quite similar in contrast to what was observed for rough silicon wafers (fig 1).

These results are confirmed by various triboscopic views made respectively out and inside the seizure area for the metal counterpart (see fig 4 arrows 3 and 4).

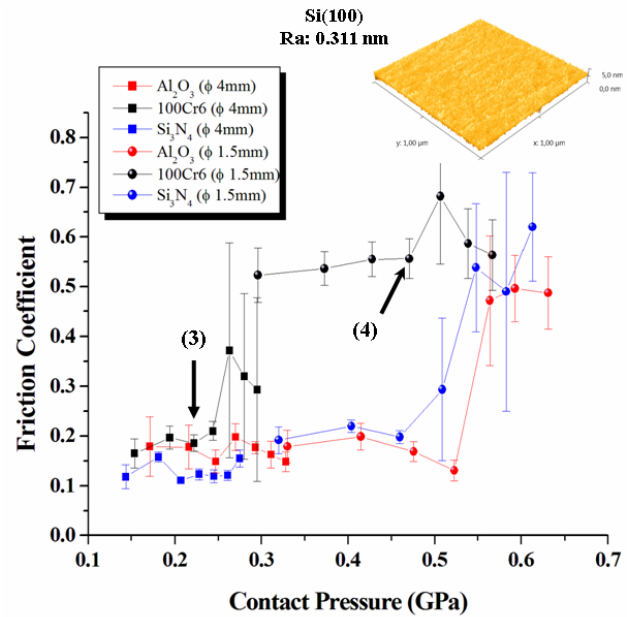


Fig 4: Variations of the friction coefficient vs. contact pressure in the case of polished monocrystal Si(100) wafers

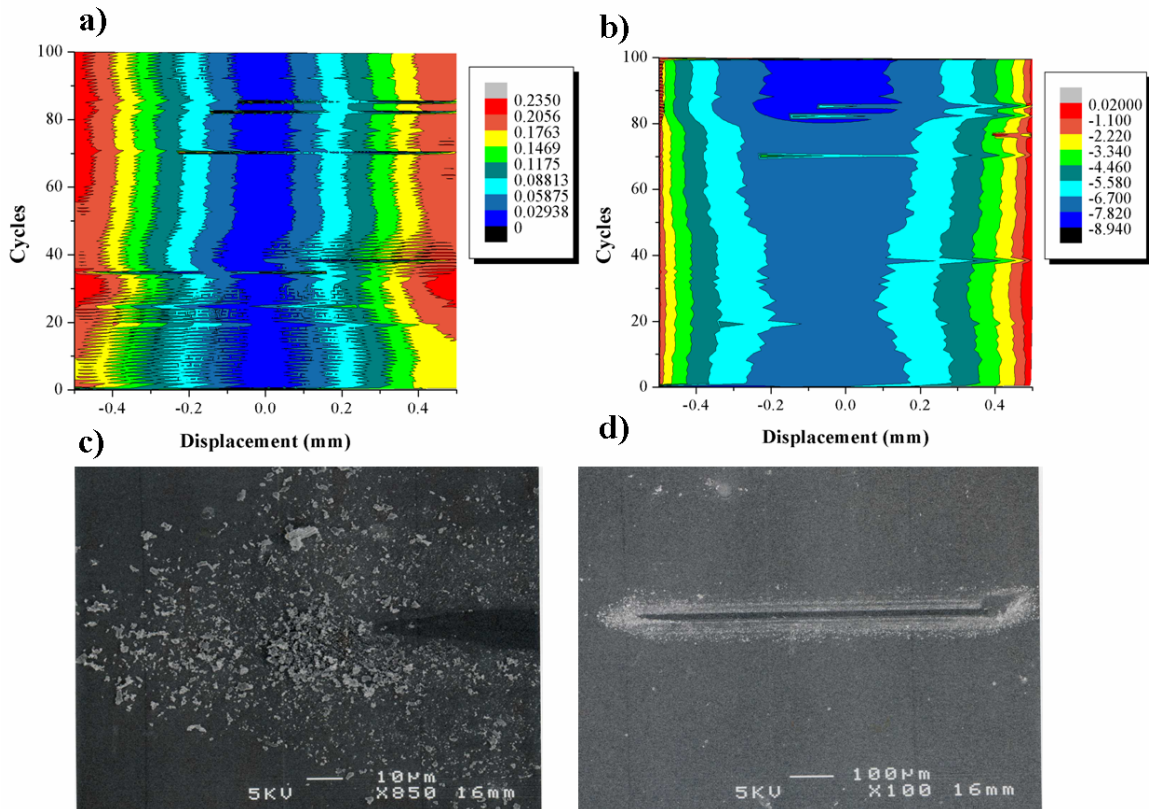


Fig 5: Triboscopic views of the test corresponding to arrow (3) in fig 4: friction map (a) ; depth map in μm (b) ; and SEM view of the wear scar end (c) and wear groove (d)

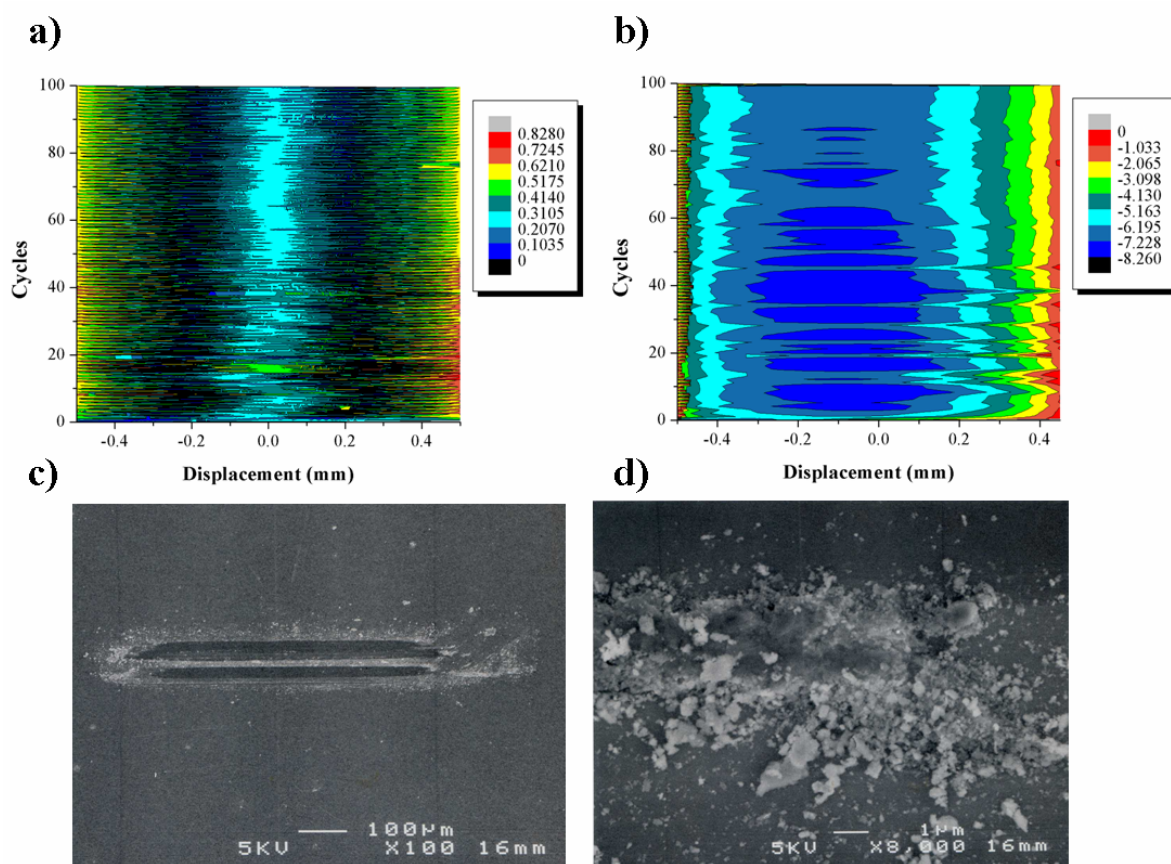


Fig 6: Triboscopic views of the test corresponding to arrow (4) in fig 4: friction map (a); depth map in μm (b); and SEM view of the wear scar (c) and wear debris spread over the groove (d)

Thus, outside the seizure area (arrow 3 shown in fig 4), fig. 5a reveals a *friction map* quite homogeneous along the friction track and with time. The *depth map* (fig 5b) reveals a regular wear rate without any wear debris within the friction groove. As shown on SEM views (5c and d), wear debris are ejected on the friction track edges and beyond the ends. Wear debris are rather small and little agglomerated.

On the contrary, inside the seizure area (arrow 4 in fig 4), the friction map is very unstable along the friction track and with time (fig. 6a) because a very cohesive third body is generated within the contact area (fig. 6b). After 100 cycles, SEM views (fig 6c – d) reveal that the third body is crushed and spread over the friction track. Few debris are ejected out the groove

As mentioned before, many works have been carried out for a better understanding of the

friction and wear of polished Si(100) wafer in mono-asperity [3,4,7,10] and multi-asperity contact [5,6, 8,15,16,22,24,28]. As expected, for mono-asperity tribological tests using AFM, the capillarity effect is significant; leading to an adhesive wear mechanism at low loads. Besides, at high loads, Bhushan [3] showed that ploughing is a dominant contribution to the friction force when the contact stresses exceed the hardness of the sample (about 9GPa).

However multi-asperity tribological tests [eg. 16], carried out with a high number of cycles, reveal that wear of Si(100) is rather controlled by its maximal shear stress (about 120MPa) instead of its hardness. In addition, Gardos [28] and Yoon *et al* [22] showed that Si (100) wafer exhibits a high adhesive friction followed by shear-induced microcracking in the trail of the sliding contact. As we do, they also observe that wear debris are smeared at the centre of the wear groove.

Referring to the work of Kim *et al* [30], Gatzen *et al* [11,29], Gardos [31] and Jaccodine [34] the single-crystal Si(111) is known to display better mechanical properties and a lower surface energy than the Si(100) one. Thus, according to the previous remarks about wear resistance controlled by both the ultimate shear stress and the adhesion contribution, Si(111) should logically have a better wear behaviour than Si(100).

3.3. Tribological tests on polished single crystal silicon (111) wafers

Fig. 7 plots the variations of the friction coefficient - after 100 cycles – as function of the contact pressure for each type of balls rubbing on polished Si(111) wafers.

Whatever the material constituting the ball, the friction coefficient remains stable with the contact pressure. In addition, no seizure is observed at any contact pressure. As reported before for the tribological test outside the seizure area (fig. 5a-b), the triboscopic views reveal a *friction map* (fig. 8a) extremely homogeneous with time; a regular wear rate without any wear debris within the friction groove is also observed (fig 8b).

In addition, the wear rate is rather weak as shown on the typical SEM view of the friction scar (fig 8c).

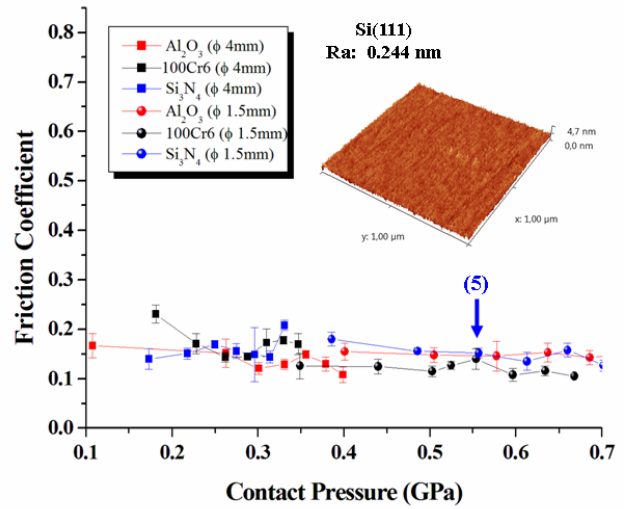


Fig 7: Variations of the friction coefficient vs. contact pressure in the case of polished monocrystal Si(111) wafers

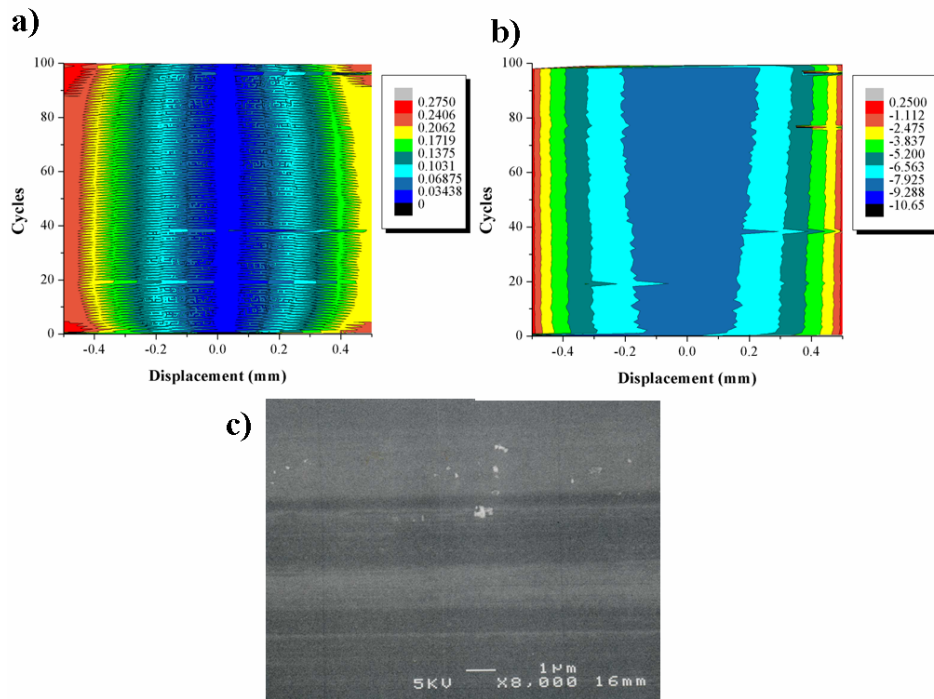


Fig 8: Triboscopic views of the test corresponding to arrow (5) in fig 7: friction map (a); depth map in μm (b); and typical SEM view of the wear groove (c)

As expected, friction and wear rate of Si(111) are strongly reduced compared to the ones of Si(100). According to Gardos [31], this behaviour can be attributed to a concomitant rise of the mechanical properties and a reduction of the adhesion contribution because Si(111) is the densest crystallographic plane of silicon. Indeed, each hydrogenated surface atom is bonded to three other atoms on (111), but only to two on (100). The force required to remove an atom from the top (111) plane is higher. Si(111) with its overall-lowest surface energy (about 1.7 times lower than Si(100)) and most firmly interwoven surface atoms producing the highest in-plane strength exhibited less cracking and wear than Si(100). Thus, the most prevalent mode of surface damage on Si(100) is tensile stress-induced microcracking normal to the direction of sliding while Si(111) exhibits mostly grain pull-out, with little evidence of cracking [31].

3.4. Tribological tests on CN₆/Si(100) and CN₆/Si(111) wafers

Carbon nitride is often mentioned for its superior mechanical and tribological properties [35, 38] similar – and even better – to those of DLC. Thus it has been shown that CN_x films deposited by sputtering and containing 10% nitrogen had better wear resistance and lower friction coefficient than pure carbon films generated under the same conditions [39]. In addition, Adachi *et al* [38] have recently reported an interesting lubricating effect of CN_x in presence of a nitrogen flow.

Fig. 9 plots the variations of the friction coefficient - after 100 cycles – as function of the contact pressure for each type of balls rubbing on CN₆ coatings deposited on polished Si(100) wafers.

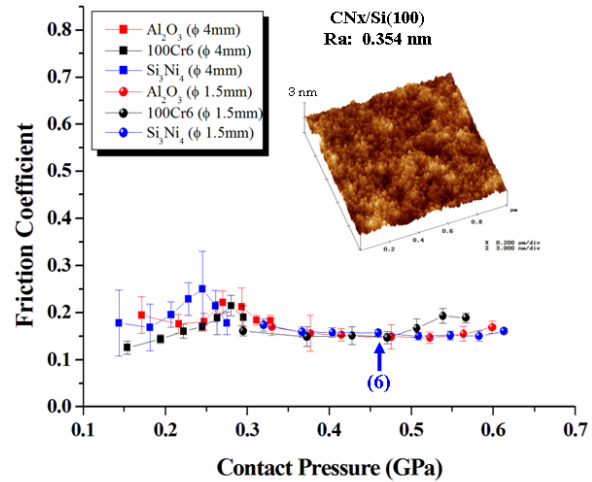


Fig 9: Variations of the friction coefficient vs. contact pressure in the case of CN₆ coatings deposited on polished monocrystal Si(100) wafers

Note that the same results have been obtained with Si(111) wafer substrates proving that the previous crystallography-induced anisotropy phenomenon in friction and seizure does completely vanish when CN_x coatings are deposited on silicon wafers. As for Si(111), the friction coefficient remains stable with the contact pressure and is rather independent of the antagonist. No seizure is observed at any contact pressure.

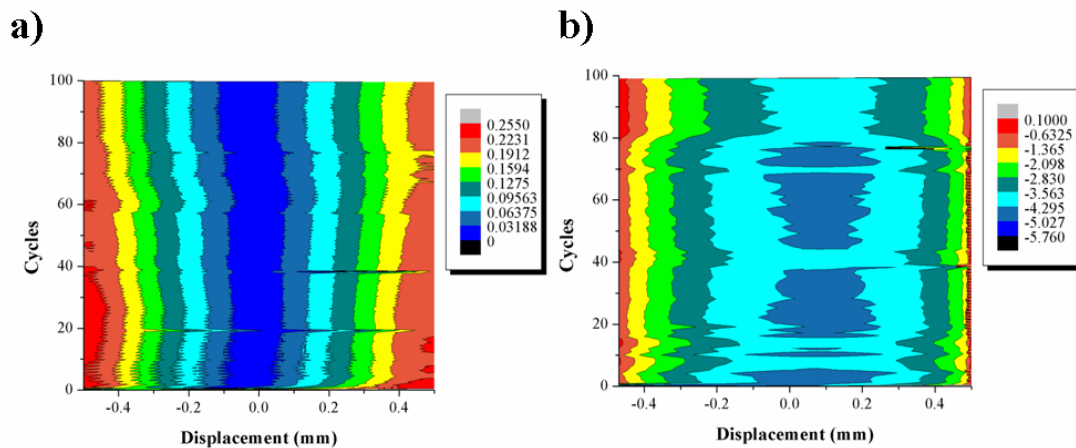


Fig 10: Triboscopic views of the test corresponding to arrow (6) in fig 9: friction map (a); depth map in μm (b)

For test (6) shown in fig 9, triboscopic views (fig. 10) reveal that the *friction map* and the *depth map* are extremely homogeneous with time. Besides, the latter reveals that a time-dependent tribolayer – probably constituted by agglomerated wear debris – is starting to build up from 80 cycles within the contact.

According to Adachi *et al* [38], this third body should have a lubricating effect in presence of nitrogen flow. In order to check this assumption, tribological tests have been carried out during 4000 cycles – corresponding to 8 meters – both in air or nitrogen (fig 11).

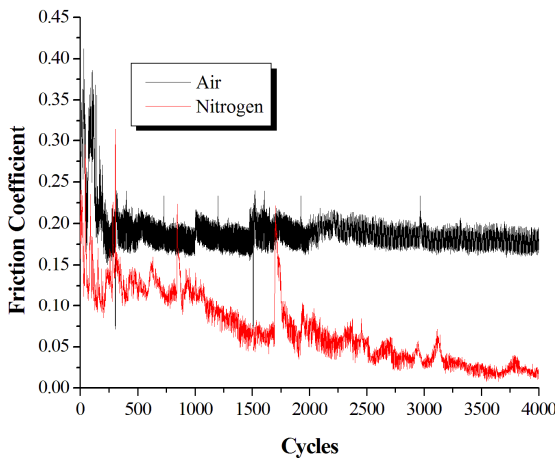


Fig 11: Evolution of the friction coefficient for $CN_x/Si(100)$ under air and nitrogen

Thus, in contrast to what is observed under ambient air where the friction coefficient remains constant around 0.17, it strongly decreases until 0.03 under nitrogen flow. With the help of Raman analysis, Adachi *et al* [38] have recently explained this decrease by the possible migration of nitrogen atoms from the gas into the lattice defects of a graphite-like structure formed in the tribolayer.

4. SUMMARY

- Friction and wear rate of Si(111) are strongly reduced compared to the ones of Si(100) due to its lowest surface energy and highest in-plane strength ;

- Roughness of bare silicon mainly influences the generation rate of the third body and controls the seizure occurrence ;
- When CN_x coatings are deposited on silicon wafers, anisotropy does completely vanish: friction and wear mechanisms are instead controlled by the surrounding environment. Thus, in presence of nitrogen flow the friction coefficient decreases from 0.2 to 0.03 due to the interaction of the gas with the third body

5. REFERENCES

- [1] Kim, S. H. *et al*, **Nanotribology and MEMS**, nanotoday, october 2007, 2, N°5, 22-29.
- [2] Achanta, S., Celis, J-P., **Nanotribology of MEMS/NEMS**, in Gnecco, E. Meyer, E., (eds) *Fundamentals of friction and Wear on the Nanoscale*, Berlin, Heidelberg: Springer-Verlag, 2007, 522-547.
- [3] Bhushan, B., **Nano-tribology and Nano-mechanics**, *Wear* 259, (2005), 1507-1531.
- [4] Bhushan, B., Koinkar, V.N., **Micro-tribological studies of doped single-crystal silicon and polysilicon films for MEMS devices**, *Sensors and Actuators A*, 57, (1996), 91-102.
- [5] Scherge, M. *et al*, **The effect of water on friction of MEMS**, *Tribology Letters*, 6, (1999),
- [6] Achanta, S. *et al*, **Investigation of friction on hard homogeneous coatings during reciprocating tests at micro-Newton normal forces**, *Wear* 263, (2007), 1390-1396. 215-220.
- [7] Xu, J.X., *et al*, **Nanofretting behaviours of monocrystalline silicon (100) against diamond tips in atmosphere and vacuum**, *Wear* 267, (2009), 322-329.
- [8] Liu, H., *et al*, **Microtribological properties of silicon and silicon coated with DLC, OTS and STCd salt films: a comparative study**, *Thin Solid Films*, 381, (2001), 135-142.
- [9] Myshkin, N., *et al*, **The effect of adhesion on sliding friction at nanoscale**, in Bartz J., Franek F (eds), *Proc. 3rd Vienna International Conference NANOTECHNOLOGY*, (2009), 323-328.
- [10] Zhao, X., Bhushan, B., **Material removal mechanisms of single-crystal silicon on**

- nanoscale and ultralow loads**, *Wear*, 223, (1998), 66-78.
- [11] Gatzert, H.H., Beck, M., **Wear of single crystal silicon as a function of surface roughness**, *Wear*, 254, (2003), 907-910.
- [12] Mate, C.M., **Tribology on the small scale**. NY: Oxford University Press, 2008, 333p
- [13] Nosonovsky M., Bhushan B., **Capillary effects and instabilities in nanocontacts**, *Ultramicroscopy*, 108, (2008), 1181-1185.
- [14] Bhushan B., **Nanoscale tribophysics and tribomechanics**, *Wear* 225-229 (1999) 465-492.
- [15] Patton, S.T., *et al*, **Effects of adsorbed water and sample aging in air on the μN level adhesion force between Si(100)**, *Tribology International*, 34, (2001), 481-491.
- [16] Nevshupa, R.A., *et al*, **Transitional microfriction behaviour of silicon induced by spontaneous water adsorption**, *Surface Science* 517, (2002), 17-28.
- [17] Meyer, E. Lüthi, R., **Tribological experiments with friction force microscopy**, in Nalwa H.S., *Handbook of Nanostructured Materials and Nanotechnology* (2000), Vol. 2, 345-383,
- [18] Szlufarska, I., *et al*, **Recent advances in single-asperity nanotribology**, *J Phys. D: Appl. Phys.* 41, (2008), 123001
- [19] Colaço R., **An AFM study of single-contact abrasive wear: The Rabinowicz wear equation revisited**, *Wear* 267, (2009), 1772-1776.
- [20] Schmutz, J-E., *et al*, **Measuring wear by combining friction force and dynamic force microscopy**, *Wear* 268, (2010), 526-532.
- [21] Scherge, M., **Scale dependence of friction**, *Proc. World Tribology Congress*, (2001), 31-37
- [22] Yoon, E-S., *et al*, **The effect of contact area on nano/micro-scale friction**, *Wear*, 259 (2005), 1424-1431.
- [23] Sung, I-H., *et al*, **Effect of surface topography on the frictional behaviour at the micro/nano-scale**, *Wear* 254, (2003), 1019-1031.
- [24] Qing, T., *et al*, **Micro-friction and adhesion measurements for Si Wafer and TiB_2 Thin film**, *Tsinghua Science and Technology*, vol. 12, N°3, (2007) 261-268.
- [25] Brendlé, M., Diss, P., Stempflé Ph., **Nanoparticle detachment: a possible link between macro-and nanotribology?**, *Tribology Letters* 9, (2000), 97-104.
- [26] Stempflé, Ph. *et al*, **Evaluation of the real contact area in three-body dry friction by μTA** , *Tribology International*, (2009), doi: [10.1016/j.triboint.2009.12.001](https://doi.org/10.1016/j.triboint.2009.12.001).
- [27] Stempflé, Ph., von Stebut, J., **Nano-mechanical behaviour of the 3rd body generated in dry friction**, *Wear* 260 (2006) 601-614.
- [28] Gardos, M.N., **Surface chemistry-controlled tribological behaviour of silicon and diamond**, *Tribology Letters*, 2, (1996) 173-187.
- [29] Gatzert, H.H., Beck, M., **Investigation on the friction force anisotropy of the silicon lattice**, *Wear*, 254, (2003), 1122-1126.
- [30] Kim, J., *et al*, **Why is (111) Silicon a better mechanical material for MEMS?**, *Euroensors XV*, 1, (2001), 662-665
- [31] Gardos, M.N., **Tribological behaviour of polycrystalline and single-crystal silicon**, *Tribology Letters*, 2, (1996), 355-373.
- [32] Hodar F., *et al*, **Microindentation de lames de silicium: influence des effets d'orientation**, in Takadoum J. (ed), *Tribologie et microsystèmes*, (2002), 85-96.
- [33] Jaccodine R.J., **Surface Energy of Germanium and Silicon**, *J. Electrochem. Soc.*, Volume 110, Issue 6, (1963), 524-527.
- [34] Takadoum, J. *et al*, **Comparative study of mechanical and tribological properties of CNx and DLC films**, *Surface & Coatings Technology*, 174-175, (2003), 427-433.
- [35] Callister, W.D., Jr, **Materials Science and Engineering**, (2000), John Wiley & Sons, 782p;
- [36] Ohmae, N., *et al*, **Micro and Nanotribology** ASME Press, (2005), New York, 185p.
- [37] Adachi, K., Kato, K., **Tribology of Carbon Nitride Coatings**, in Donnet C., Erdemir A., (eds), *Tribology of Diamond-like Carbon Films*, Springer, (2008), 339-361.
- [38] Khurshudov, A., *et al*, **Tribological and mechanical properties of carbon nitride thin coating prepared by ion-beam-assisted deposition**, *Tribology Letters*, 2, 1, (1996), 13-2